International Journal of Hydrogen Energy 126 (2025) 439–449

Contents lists available at ScienceDirect

International Journal of Hydrogen Energy

journal homepage: www.elsevier.com/locate/he

Separation of hydrogen-methane mixtures by electrochemical hydrogen compressor: Experimental and modelling investigation on the influence of different Nafion membranes and operative conditions

Elisa Zanella [a,*], Mariangela Longhi [a], Giacomo Tondelli [a], Alessandro Minguzzi [a,b,c], Antonio Comite [d], Alberto Vertova [a,b], Carlo Pirola [a,b]

[a] Dipartimento di Chimica, Università degli Studi di Milano, via Golgi, 19, 20133, Milano, (MI), Italy
[b] Istituto Nazionale di Scienza e Tecnologia dei Materiali, via Giusti 9, Firenze (FI), Italy
[c] Dipartimento di Energia, Politecnico di Milano, Via Lambruschini, 4a, 20156, Milano, (MI), Italy
[d] Department of Chemistry and Industrial Chemistry, Università di Genova, 16146, Genova, (GE), Italy

ARTICLE INFO

Handling Editor: Ramazan Solmaz

Keywords:
Electrochemical hydrogen compressor
Hydrogen
Methane
Nafion
Separation
Modelling

ABSTRACT

The electrochemical hydrogen compressor (EHC) offers an effective solution for hydrogen transport challenges, enabling simultaneous purification and compression, even when hydrogen is blended with natural gas at low concentrations. This study investigates the impact of three commercial Nafion® membrane types (Nafion® 117, Nafion® 115, and Nafion® 212) on the separation efficiency of EHC, examining the influence of temperature, methane concentration, and hydrogen flow rate, thereby providing a comprehensive evaluation of membrane-specific performance on the EHC's efficiency. Nafion® 212 demonstrated superior energy efficiency due to its lower thickness and higher ion-exchange capacity. Tests with a 90:10 methane:hydrogen molar ratio revealed an energy consumption of 2.30 kWh·kg^{-1}H$_2$ and hydrogen purity exceeding 99 %. The experimental results were validated with a mathematical model incorporating key parameters from existing literature, achieving an average deviation of 2.5 % between the model and experimental data.

1. Introduction

In our modern world, where energy demand is always rising and worries about climate change are growing [1], the imperative to shift towards renewable energy sources has never been more urgent. Renewable energies can drive decarbonization, but efficient storage is key to ensuring stability and unlocking their full potential for a sustainable future [2]. In this regard, hydrogen seems to be very promising as energy vector, due to its exceptionally high gravimetric energy density [3]. However, hydrogen's industrial utilization is hindered by its high flammability and low volumetric energy density, which make it very difficult to store and transport [4].

In recent years, it has been agreed that a possible solution could be the transport of hydrogen through pipes, as has been the case for natural gas for decades. This would allow in transport and diffusion of hydrogen produced in a green manner from large production sites to the entire supply chain concerned. The hydrogen transported in these pipelines can be pure or blended with natural gas, so as to exploit the existing network. In this regard Europe countries with the European Hydrogen Strategy (2020) [5] decided to increase the quantity of hydrogen in the European energy mix, now below 2 %, to 13–14 % by 2050. As a result of this proposal some states have implemented for the realization of hydrogen pipelines, the European Hydrogen Backbone targeting 27.000 km of pipelines in 2030 and 53.000 km in 2040 [6].

Pure hydrogen in pipelines can be directly utilized for power generation, transport, and industrial applications. However, when blended with natural gas, it poses challenges related to separation, purification, and storage after grid transport. The separation of hydrogen from methane is crucial in various industrial applications. In addition to the above-mentioned specific case of deblending from natural gas pipelines, this separation is essential in hydrogen production via steam methane reforming (SMR) and autothermal reforming (ATR) [7,8]. Additionally, hydrogen purification is required in ammonia and methanol synthesis, underground hydrogen storage, and emerging methane pyrolysis technologies [9]. Efficient separation processes are generally key to ensuring high-purity hydrogen for industrial and energy applications. Usually,

* Corresponding author.
E-mail address: elisa.zanella@unimi.it (E. Zanella).

https://doi.org/10.1016/j.ijhydene.2025.04.014
Received 10 January 2025; Received in revised form 28 February 2025; Accepted 1 April 2025
Available online 11 April 2025

Table 1
Summary of published articles on electrochemical hydrogen separation from methane-hydrogen mixture.

	Catalysts	Membrane	Gas Diffusion Layer	Active area (cm^2)	Temp. (K)	Ref.
Ibeh et al., 2007	Pt/C, Pt–Ru/C	Nafion® 115	–	25	293–343	[35]
Onda et al., 2007	–	–	–	10	–	[36]
Perry et al., 2008	Pt/C	PBI	–	10	433	[28]
Doucet et al., 2009	Pt/C	Nafion® 115	–	25	298	[37]
Thomassen et al., 2010	–	PBI	–	3.25	433–453	[38]
Nordio et al., 2019	Pt/C	Nafion® 212	–	50	≤301	[39]
Jackson et al., 2020	Pt/C, Pt–Ru/C	Nafion® 212	Sigracet SGL 28BCE™	5	308	[34]
Vermaak et al., 2021	Pt/C and Pt–Co/C	TPS®-based	–	25	373–433	[40]
Jackson et al., 2024	PtRu/C and Pt/C	Nafion® 117	Sigracet SGL 29 BCE	25	308	[12]
This work	Pt/C	Nafion® 117, Nafion® 115, Nafion® 212	Carbon Cloth with MPL - W1S1011	10	293–323	–

the industrial separation of hydrogen is mainly performed using Pressure Swing Adsorption (PSA). Currently, about 85 % of the produced hydrogen is purified by PSA [10]. However, this technique has a low hydrogen recovery and, if H_2 in the stream is lower than 40 %, it is economically unfeasible [11]. Indeed, PSA units are ideal for high inlet concentrations of H_2 and for large scale plant. It has reported an energy consumption of ~3.3 kWh·$kg^{-1}H_2$ for the separation of 30 % H_2 in CH_4, increasing to ~20 kWh· $kg^{-1}H_2$ for 10 % H_2 in CH_4 [12]. Besides PSA, membranes offer an alternative solution, some examples are: metal-based membrane, particularly Pd-based or Pd alloys [13], carbon-based membrane [14] and polymeric membranes [15]. However, their high capital cost, driven by the large surface area required for high fluxes due to permeability and pressure constraints, limits their feasibility [13]. For this reason, it is necessary to study different technologies that permit the separation of hydrogen from the blended grid.

In this work, the Electrochemical Hydrogen Compressor (EHC) is taken into consideration for the separation of hydrogen in low amount, down to 10 %, in a methane-hydrogen mixture. In fact, since its first publication in 1998 by Rohland et al. [16], it has been possible to appreciate the great potential of this technology, that is to combine separation and compression of hydrogen in a single device due to the electrochemical principle on which it is based, namely, the hydrogen oxidation reaction (HOR) from an impure stream at the anode and the evolution of pure, high-pressure hydrogen at the cathode (HER: Hydrogen Evolution Reaction) [17]. Obtaining pure hydrogen at the outlet requires a minimum electrical work to drive the following reactions:

$$\text{Anode}: H_2 \rightarrow 2H^+ + 2e^- \quad \text{Eq. 1}$$

$$\text{Cathode}: 2H^+ + 2e^- \rightarrow H_2 \quad \text{Eq. 2}$$

whose Nernst equation [18] is:

$$E = E^0 + \frac{R_{gas}\,T}{2F} ln\left(\frac{p^{H_2}_{Cathode}}{p^{H_2}_{Anode}}\right) \quad \text{Eq. 3}$$

where E^0 is the cell potential at standard conditions (0.000 V in the case of above described reactions), R_{gas} is the gas constant (8.314 J mol^{-1} K^{-1}) and F is Faraday's constant (96485 C mol^{-1}).

According to this equation, a potential differential of only 0.054 V is enough to increase the hydrogen pressure from 1 (p_{anode}) to 70 MPa ($p_{cathode}$) at room temperature [17]. However, this potential value is strictly connected to an equilibrium condition. When the EHC works, a higher potential must be applied due to both anodic and cathodic overpotentials, directly connected with electrode materials, Ohmic losses, mainly due to electrolyte between the two electrodes, and mass transfer limitations [19]. Thus, Equation (3) becomes:

$$U_{cell} = E + \eta_{ET} + Ri = E^0 + \frac{R_{gas}\,T}{2F} \ln\left(\frac{p^{H_2}_{Cathode}}{p^{H_2}_{Anode}}\right) + \eta_{ET} + Ri \quad \text{Eq. 4}$$

where U_{cell} is the experimental cell potential, η_{ET} is the sum of both anode and cathode Electron Transfer overpotential; R sum up the Ohmic losses and i is the current.

The core of EHC is the membrane electrode assembly (MEA), that is based on two gas diffusion electrodes (GDEs) and a proton exchange membrane (PEM) [16]. The key factor influencing the performance of EHC systems is the membrane, as it determines both electrical resistance and proton conductivity. Consequently, a membrane with superior ionic conductivity is essential to minimize Ohmic losses. Furthermore, the membrane must exhibit strong mechanical, thermal, and chemical stability to withstand operational conditions [20,21]. The catalyst layer also plays a crucial role in lowering the activation energy of electrode reactions. Platinum is widely recognized for its excellent catalytic activity in EHC processes and is frequently referenced in research; however, its performance can be compromised due to the poisoning of active sites by impurities, especially CO, CO_2, and H_2S [22]. For this reason and with the aim of reducing the costly noble metal, other composite materials have been studied and proposed [23], also to possibly reduce the environmental impact of their production [24].

Rhandi et al. [19] demonstrated that the EHC has many advantages: high gas recovery, compatibility of the process with continuous operation, low energetic cost thanks to the minimal electric work for the purification, and high purity of hydrogen, even higher than 99.9 % [22]. In addition, the low operating temperatures, comprised between room temperature and 498 K, are very convenient for the material durability and sealing system [21]. This system is also compatible with small units of purification, which render them well-suited for fuel cell vehicles refilling systems [25]. However, industrial-scale progress has been limited by issues such as the high mechanical stress from large pressure differences, particularly affecting the thin PEM structure [19]. Another limitation of the use of polymer membranes is the possible diffusion of gases through them. This phenomenon is witnessed by a loss of system efficiency in the case of hydrogen back-diffusion from high pressure cathode to low pressure anode, and in a diffusion by permeation of pollutants from the anode to the cathode, that will affect the purity of hydrogen [18,26]. Moreover, membrane hydration, water and thermal management are other important critical issues that must be considered [27].

In general, EHCs can be classified as low-temperature EHCs, working with low-temperature PEMs as membranes (e.g. Nafion®, SPEEK: sulfonated poly(ether ether ketone)) [21], high-temperature EHCs with high-temperature PEMs as membranes (e.g. acid-doped PBI: polybenzimidazole) [28], and solid oxide EHCs with perovskite-type oxides as membranes [25]. Indeed, the operating temperature of EHCs is heavily influenced by the performance of the membranes.

In this study, a low-temperature EHC with Nafion® membrane and Pt catalyst was investigated and tested in hydrogen separation from different methane-hydrogen mixtures. In literature, it has been documented that EHCs can separate H_2 from various mixtures with other compounds, including CO_2 [29], CO [30], N_2 [31], Ar [32], NH_3 [33], and H_2S [34]. Regarding the separation from CH_4, a summary of published articles on electrochemical hydrogen separation are reported in Table 1, focusing the attention on the catalysts and membranes used for

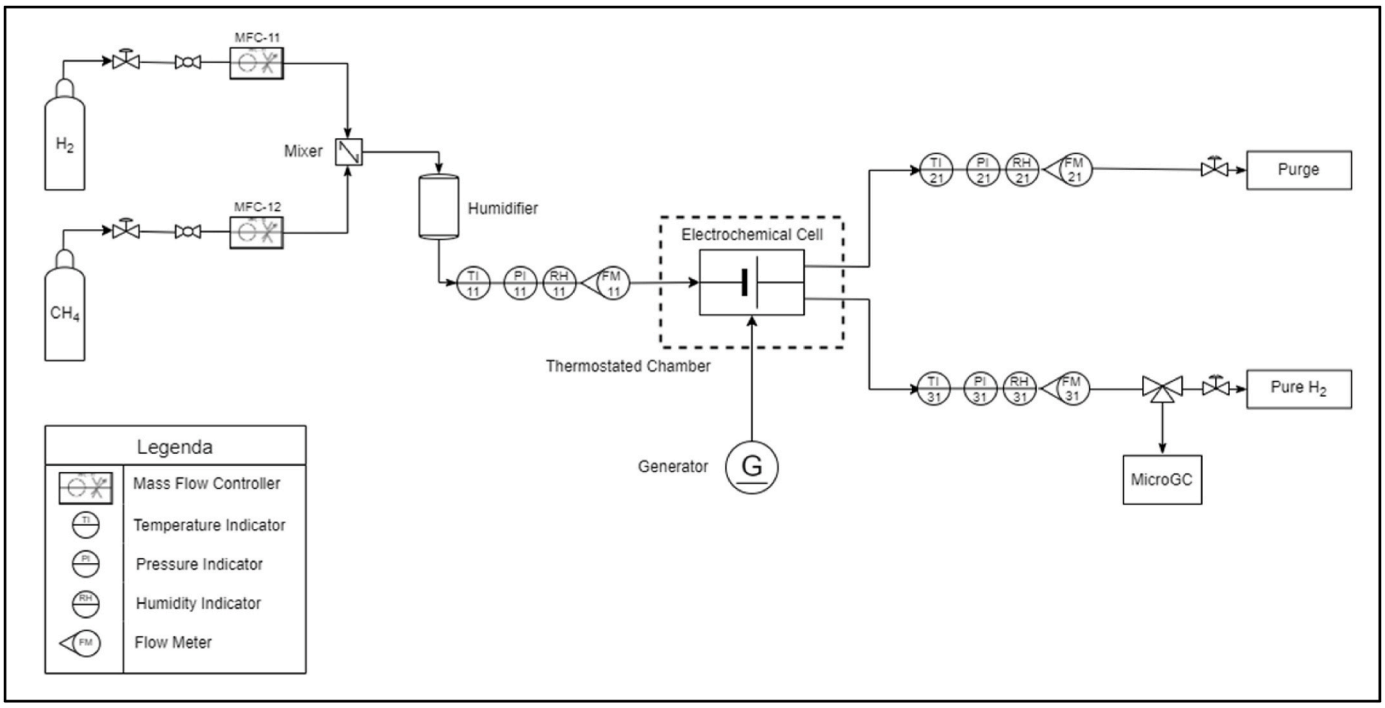

Fig. 1. Bench scale laboratory plant used for the EHC tests.

the experimental tests, and also on the working temperature.

Nafion® is often preferred over other membranes due to its high proton conductivity, excellent chemical stability, and proven performance in a wide range of electrochemical applications, making it particularly suitable for processes like electrochemical hydrogen compression, where reliable and efficient ion conduction is crucial [41]. The main technical challenges that arise from literature studies on this polymer include degradation under prolonged operation, reduced proton conductivity at low humidity levels, and variations in mechanical stability that affect long-term performance [39]. Furthermore, differences in membrane thickness and equivalent weight significantly impact hydrogen crossover and energy efficiency [41]. With a focus on three distinct Nafion® membrane types that are frequently employed for this class of electrochemical devices — Nafion® 117, Nafion® 115, and Nafion® 212 — this work carefully examined the impact of membrane type and its properties on the purifying efficiency by EHC. Additionally, the effects of temperature, the amount of methane in the mixture, the flow of hydrogen, and the level of purity obtained were examined. In contrast to previous studies that focus on a single membrane type, this work examines a variety of MEAs under identical operational conditions. This approach allows for a true comparison of membrane-specific behaviours, providing a deeper and more comprehensive understanding of performance differences across membrane types on the efficiency of EHC device. In addition, since there are several publications on EHC computational simulations and mathematical models [39,42–44], but not all were validated with experimental data, it was decided to validate the experimental results with a mathematical model. The model uses data from most of the relevant studies on the topic, focusing on performance evaluation by simulating the state and conditions across the entire active surface of the cell. Moreover, the model focuses on the material balance between the two sides of the cell, taking in consideration the permeation of gasses through wet Nafion® from the experimental results for the final purity, as well as the efficiency from the back-diffusion of hydrogen, the humidification of the membrane and the water transport. For the current-potential correlation the dependencies on membrane physical and chemical features, temperature, hydrogen concentration and membrane water content in the working conditions were considered.

2. Materials and methods

2.1. Description of the set up

The electrochemical cell utilized in this study consists of two plastic end plates, two copper current collectors, and two closed bipolar graphite plates featuring a serpentine flow field. This flow field, designed with eight parallel channels, facilitates gas diffusion and has a depth of 0.75 mm and a total length of 30 mm per flow field. The assembly is sealed using PTFE gaskets. At the core of the cell lies the membrane electrode assembly (MEA), which is a commercially available 5-layer structure with an active area of 10 cm^2, supplied by Fuel Cell Store Company. The MEAs incorporate two Carbon Cloth Gas Diffusion Layers (GDL), two Pt/C catalyst layers, and a proton exchange membrane. The three tested MEAs differ by the type of membrane: Nafion® 117, Nafion® 115 and Nafion® 212 respectively for MEA 1, MEA 2 and MEA 3. The catalyst amount and composition were maintained constant for all the MEAs tested at 0.3 mg cm^{-2} (20 % Pt) and 0.5 mg cm^{-2} (60 % Pt) of loaded Pt/C respectively for the anode and cathode sides.

The cell was inserted in a jacketed thermostated chamber to ensure stable and controlled operating conditions. The supplied anode inlet gas is a mixture of methane and hydrogen. The composition of the H_2:CH_4 mixture fed to the anodic chamber is prepared by two mass flow controllers (by Brooks), which have a maximum volume flow rate of 100 NmL·min^{-1} and 20 NmL·min^{-1} respectively for methane and hydrogen. To regulate membrane hydration, the gases were humidified before entering the anode chamber via a system consisting of a temperature-controlled flask filled with ultra-pure water through which the gases are bubbled. Key operating parameters, including pressure, temperature, and humidity, were monitored using WIKA, TC Direct, and MICHELL instruments, respectively, for the inlet, outlet, and purge streams. Flow rates of the purge and outlet streams were measured with a bubble flowmeter to assess system efficiency and mass balance. An Elind DC, series HL, power supply with an applicable potential between 0 and 150 V and an applicable current between 0 and 4 A has been used.

At the end of the plant an Agilent 3000 MicroGC from Agilent Technologies equipped with PLOT Q and MoleSieve 5A as first and second column was used for analytical determinations [45]. The general layout of the plant is schematized in Fig. 1.

2.2. Separation tests

Separation tests have been performed using the following procedure. At different fixed temperatures and atmospheric pressure, the gas mixture has been humidified and fed in the cell anodic chamber maintaining a constant hydrogen inlet flow of 10 NmL·min^{-1}. The cell potential (U_{cell}) has been monitored, while current values between 0 and 1.5 A have been applied to the cell, to determine the resistance and the associated overvoltage of the system. The purity of the output gas has been checked using the microGC. When the flux of anodic H_2 is major or equal to the relative current, as defined in Equation (5).

$$\dot{n}_{H_2 \text{anodic (or cathodic)}}\left(\text{mol min}^{-1}\right) = \frac{i(\text{C s}^{-1})\cdot 60\left(\text{s min}^{-1}\right)}{2\cdot F\left(\text{C mol}^{-1}\right)} \quad \text{Eq. 5}$$

where $\dot{n}_{H2}$ is the hydrogen flux in anodic chamber, i is the applied current and F is Faraday's constant (96485 C mol^{-1}), the consumed H_2 (chemical reaction 1) is equal to the produced one in cathodic chamber (chemical reaction 2). When H_2 flux in anodic chamber is less than the applied current, the hydrogen production flux in cathodic chamber is still defined by Equation (5), but a cathodic parasitic reaction is present to sustain the current: the water oxidation.

$$2H_2O + 2e^- \rightarrow H_2 + 2OH^- \quad \text{Eq. 6}$$

This reaction not only modifies E^0 of Equation (3), thus modifying E, but also dehydrates cationic membrane thus increasing the U_{cell}, leading to an electrolytic process with an almost 100 % current efficiency, but with an increase of the energy consumption, due to the increase of U_{cell}.

The system reaches a flux limited condition, thus evidencing a flux limited current, i_{FL}:

$$i_{FL} = \frac{2\cdot F\left(\text{C mol}^{-1}\right)\cdot \dot{n}_{H_2,\text{anodic}}\left(\text{mol min}^{-1}\right)}{60\ \left(\text{s min}^{-1}\right)} \quad \text{Eq. 7}$$

Firstly, the membranes were tested with pure hydrogen to study the influence of its flowrate. Then, the three different Nafion® membranes were tested and their performance in presence of hydrogen and methane-hydrogen mixtures were investigated, comparing the resistance and the energy consumptions.

A more detailed study was done on the Nafion® 212 membrane. The influence of the quantity of Pt in the anode side catalyst was evaluated. In a second phase, the separation of hydrogen from a mixture was studied with different methane:hydrogen molar ratios, ranging from 10:90 to 90:10, evaluating the efficiency of the system and the purity of the hydrogen obtained. Since it is known that the ionic conductivity of Nafion® increases with temperatures up to a maximum of around 333 K [46], the influence of this parameter was also evaluated. The two mixtures with the higher quantity of methane, namely 70:30 and 80:20 methane:hydrogen molar ratio, were investigated changing the temperature from 293 to 323 K. Finally, a stack of two and three cells was assembled and investigated, to explore the effects of numbering up the process. In this configuration, the single units are placed electrically in series and in parallel with respect to the gas flow.

2.3. Permeation tests

To evaluate the permeation of the impurities, particularly methane, through the Nafion® membrane, specific permeation tests were performed. In detail, the permeability of dry and wet Nafion® 212 was studied using a 90:10 methane:hydrogen mixture as the inlet gas, to mimic the worst conditions under which the separation experiments can be carried out. 100 NmL·min^{-1} of this mixture was flowed inside a cell containing a membrane with an active area of 2.83 cm^2. The inlet pressure was set at 2 barg, while the other side at 0 barg. The permeate flow was evaluated using a GC (Agilent 7890) in line equipped with a TCD detector. A minimum flow of N_2, namely 2 NmL·min^{-1}, was continuously fed into the permeate side as sweep gas to allow the permeate to reach the analytical instrument.

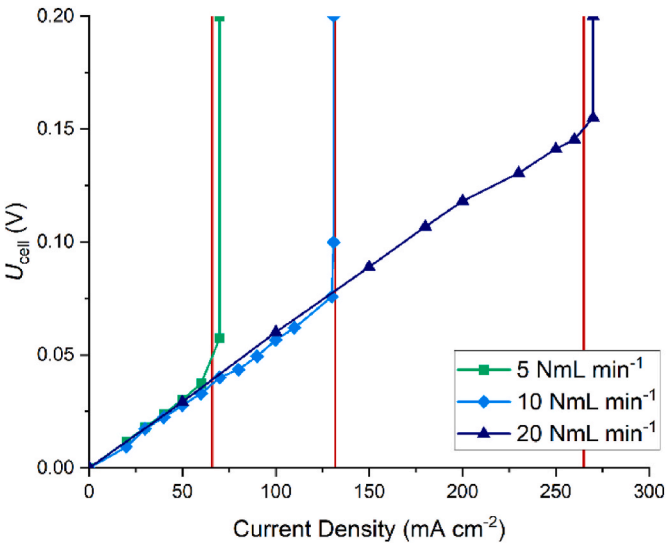

Fig. 2. Polarization curves at different hydrogen inner flowrates. The calculated i_{FL} for each hydrogen flow (red vertical line) are: 66, 132 and 263 mA cm^{-2}. Process conditions: ambient pressure for both cathode and anode, 298.15 K, hydrogen inner flow 5, 10 and 20 NmL·min^{-1}, humidity of the gas constant at 100 %. (For interpretation of the references to colour in this figure legend, the reader is referred to the Web version of this article.)

3. Results and discussion

3.1. Influence of hydrogen inner flow

To evaluate the influence of H_2 anodic flowrate on the electrochemical cell behaviour, in term of U_{cell}, pure H_2 was fed to the anodic chamber, and the amount of purified hydrogen (cathodic chamber) was sampled to verify that the production rate was as described in Equation (5). Indeed, this equation permits to calculate the theoretical moles of hydrogen that pass through the cell per minute, depending on the selected current, as previously described. To investigate the variation of U_{cell} with H_2 anodic flux, three different hydrogen inner flowrates were tested, namely 5, 10 and 20 NmL·min^{-1}, and the associated polarization curves are reported in Fig. 2.

As described by Equation (4) the total cell potential is a sum of different parameters. Depending on the current density, one of these limitations dominates. At low current density, charge-transfer limitations, specifically activation overpotential, predominate. In the intermediate region, the cell internal resistance becomes the dominant factor, and it is primarily attributable to the non-infinite conductivity of the proton-exchange membrane and electrode materials (e.g., current collectors, bipolar plates, GDLs, etc.) and contact resistance related to the interfaces between the various layers. Since the membrane typically has the greatest influence on R, it is frequently the only loss that is considered in the literature [21]. In the region of high current density, the depletion of reactants, limits the overall cell reaction rate [39]. These kinetics limitations increase when the current density increases, which means that the energetic efficiency of an EHC decreases when its productivity, namely quantity of H_2 purified, increases [19]. In this case, three different values of flux limited current were reached, see Fig. 2, corresponding to the moment when anodic H_2 flux is less than applied

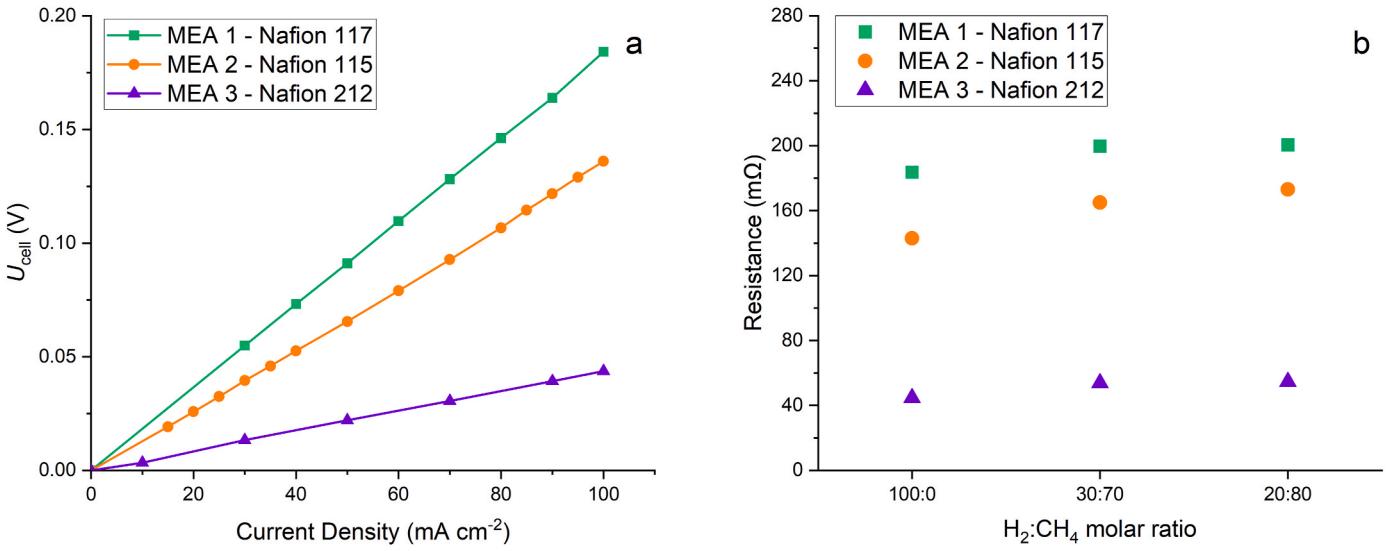

Fig. 3. a) Polarization curves for the tested MEAs with pure hydrogen. b) Nafion®'s electrical resistance obtained from polarization curves (see Fig. S1). Process conditions: atmospheric pressure for cathodic and anodic chambers; 298.15 K; hydrogen inner flow 10 NmLmin^{-1}; humidity of the gas 100 %.

Table 2
Comparison of the characteristics of the three Nafion® membranes used for the tests [47,48].

	Nafion® 212	Nafion® 115	Nafion® 117
Thickness, μm	50.8	127	183
Basis weight, g m^{-2}	100	250	360
Equivalent weight, kg mol^{-1}	1.0 ± 0.5	1.1	1.1
Dry membrane density, kg m^{-3}	1970	1980	1980
Water content, %	5.0	5.0	5.0
Water uptake, %	50.0 ± 5.0	38	38
Ion-exchange capacity, meq g^{-1}	0.92	0.90	0.90

current, as defined in Equation (7). In Fig. 2 the theoretical flux limited currents corresponding to the relevant flowrate are reported. The calculated i_{FL} from Equation (7), using the 5, 10 and 20 NmL·min^{-1} anodic gas flow rates, are: 66, 132 and 263 mA cm^{-2}.

To evaluate the influence of Pt amount in the Pt/C electrode, MEA 3 was also compared with a membrane electrode assembly that presents less amount of precious noble metal in the anode catalyst, namely 13 % instead of 20 %. The obtained polarization curves with both MEAs are comparable (see Supplementary Materials S1) and the lower amount of Pt in the catalysts layer does not significantly affect the cell performance. This suggests the possibility of further reduce the amount of noble metal in the MEA, thus lowering system costs without compromising cell performance and energy efficiency. However, it is important to acknowledge that the influence of platinum content on cell performance depends on multiple factors, including charge transfer resistance and catalyst particle dispersion. Therefore, any further reduction in the amount of precious metal should be preceded by a comprehensive study to assess its impact on overall system performance.

Table 3
Cell potential, efficiency and energy consumption for the three MEAs. Condition: 100 mA cm^{-2}, 80:20 methane-hydrogen molar ratio.

	U_{cell} (mV)	ϕ_{energ} (%)	ϕ_{prod} (%)	Energy consumption (kWh·kg$^{-1}H_2$)
MEA 1	214	9.67	99.4	5.72
MEA 2	194	10.7	99.2	5.19
MEA 3	71.5	29.0	98.0	1.94

3.2. Comparison between MEA 1, MEA 2, MEA 3

Three MEAs, prepared using three different Nafion®, were tested at 298 K with 10 NmL·min^{-1} H_2 flowrate, saturated with water and the obtained polarization curves are shown in Fig. 3a.

At the same conditions, Nafion® 212 presents the less Ohmic resistance, mainly due to its thickness, higher ion-exchange capacity and water uptake (see Table 2). Indeed, the resistance of the membrane can be calculated using the following equation:

$$R_{Mem}(\Omega) = \frac{1}{\sigma(\mathrm{S\ cm^{-1}})} \frac{L\ (\mathrm{cm})}{A(\mathrm{cm^2})} \qquad \text{Eq. 8}$$

where σ is the specific conductivity of the membrane and L and A are respectively the thickness and the area of the membrane.

Moreover, the electrochemical separation of hydrogen was evaluated using two anodic mixtures with a high quantity of methane, namely 70:30 and 80:20 methane:hydrogen molar ratio. These tests were performed maintaining a constant inner flow of hydrogen of 10 NmLmin^{-1} and increasing the quantity of methane from 0 to 40 NmLmin^{-1}. The calculated resistances are presented in Fig. 3b and they are obtained from the slopes of polarization curves (see Supplementary Material Fig. S2).

Besides the impact of the membrane type, the resistance increases with the increase of methane amount in the anodic stream. This effect is attributed to the gradual depletion of hydrogen along the active area, driven by its migration to the cathode chamber. This depletion results in a non-uniform distribution of reactants, which subsequently induces localized mass transport limitations. This phenomenon results in an increased overpotential, and consequently U_{cell}.

After having verified that the current efficiency was also around 100 %, checking the cathodic gas outlet flow rate, the energy efficiency, the production efficiency and the energy consumption were calculated by means of equations (9) and (10), respectively:

$$\phi_{energ} = \frac{2FE}{2FU_{cell}} = \frac{E}{U_{cell}} \qquad \text{Eq. 9}$$

$$W\ (\mathrm{Wh \cdot kg^{-1}}) = \frac{2\,F\ (\mathrm{C{\cdot}mol^{-1}}) \cdot U_{cell}\ (\mathrm{V})}{\phi_{prod} \cdot MM_{H2}\,(\mathrm{kg{\cdot}mol^{-1}}) \cdot 3600\ (\mathrm{s{\cdot}h^{-1}})} \qquad \text{Eq. 10}$$

where ϕ_{prod} represents the production efficiency, calculated by comparing the experimental output flow to the theoretical value. In this

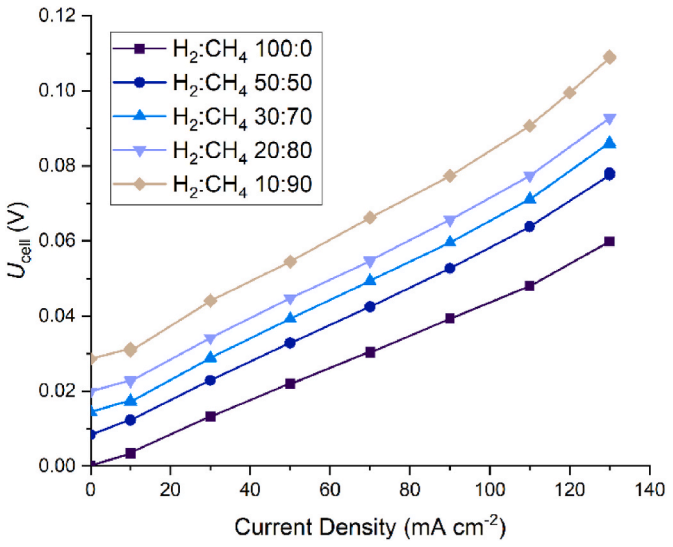

Fig. 4. Polarization curves of MEA 3 at different methane:hydrogen molar ratio. Process conditions: ambient pressure for cathode and anode; 298.15 K; hydrogen inner flow 10 NmL·min^{-1}; humidity of the gas constant at 100 %.

way, the energy consumption values account for the back-diffusion of hydrogen from the cathodic to the anodic chamber. This phenomenon is driven by the hydrogen permeability in the Nafion membrane and the Δp_{H2} between the two chambers. It is worth noting that while Nafion® 212 shows a lower resistance and energy consumption, its back diffusion is higher than Nafion® 117, as discussed later [18].

Table 3 reports U_{cell}, ϕ_{energ}, ϕ_{prod} and energy consumption for the three different MEAs, investigated at 298.15 K with a 100 mA cm^{-2} density current, using an 80:20 gas mixture ratio of methane:hydrogen. It is clear the higher energy efficiency for MEA 3, which corresponds to a lower energy consumption, due to lower resistance of the Nafion® 212.

In conclusion, the key factors influencing the system's efficiency are membrane thickness, conductivity, and water content. By analysing three similar membrane types, it was possible to identify thickness as the most critical parameter in this specific case. Under the same water content and process conditions, the N-212 membrane exhibits the lowest energy consumption compared to the other two. This can be attributed to its reduced thickness of 50.8 μm, in contrast to 127 μm and 183 μm for the N-115 and N-117 membranes, respectively.

3.3. Influence of methane-hydrogen molar ratio

Using the best performing MEA, MEA 3, the influence of anodic gas mixture ratio on the cell performance was investigated. Hydrogen: methane gas mixtures, whose molar ratios ranged from 100:0 to 10:90, were fed to the anodic chamber maintaining a hydrogen inner flow of 10 NmL·min^{-1} and the polarization curves are presented in Fig. 4.

It is evident that, as the amount of methane in the anodic stream increases, so does the system's resistance, as indicated by the increasing slope of the polarization curve. Notably, the U_{cell} at zero current (equilibrium condition) is equal to E, defined in Equation (3).

Feeding the anodic chamber with a gas mixture of 90:10 methane: hydrogen molar ratio results in a slight increase in energy consumption. At ambient pressure for cathode and anode, 298.15 K, hydrogen inner flow 10 NmL·min^{-1}, humidity of the gas constant at 100 % and current density equal to 100 mA cm^{-2}, the energy consumption calculated increases from 1.20 kWh·kgH_2^{-1} for pure hydrogen inner flow to 2.30 kWh kgH_2^{-1} when the hydrogen is purified from a gas mixture of 90:10 methane:hydrogen molar ratio. This value is consistent with those reported in the literature and significantly less than those tabulated for PSA, which is about 20 kWh kgH_2^{-1} [12].

For each test, the hydrogen purity in the cathodic chamber was quantified to evaluate the effect of increasing the methane amount in the anodic gas mixture. The study highlighted the increase of methane quantity in the purified hydrogen cathodic stream, up to a maximum percentage of 0.55 % when methane:hydrogen ratio of 90:10 was used, confirming the good separation efficiency of the system. However, this value is not enough to meet the regulatory values for fuel cells, which ask for a CH_4 content of less than 100 ppm [49]. Methane can cross the cationic membrane due to its permeability in Nafion® [50]. In literature are presented some studies related to this phenomenon [26,51,52]. However, they present only the permeability coefficients in dry Nafion®, which are not in accordance with the methane permeation experimentally observed. For this reason, a study on dry and wet Nafion® was conducted. Regarding hydrogen, a permeability coefficient of 10.08 barrer and 195.2 barrer were calculated for dry and wet Nafion® respectively. Similarly, a value of 0.72 barrer and 51.8 barrer were obtained for methane, confirming the enhanced permeability due

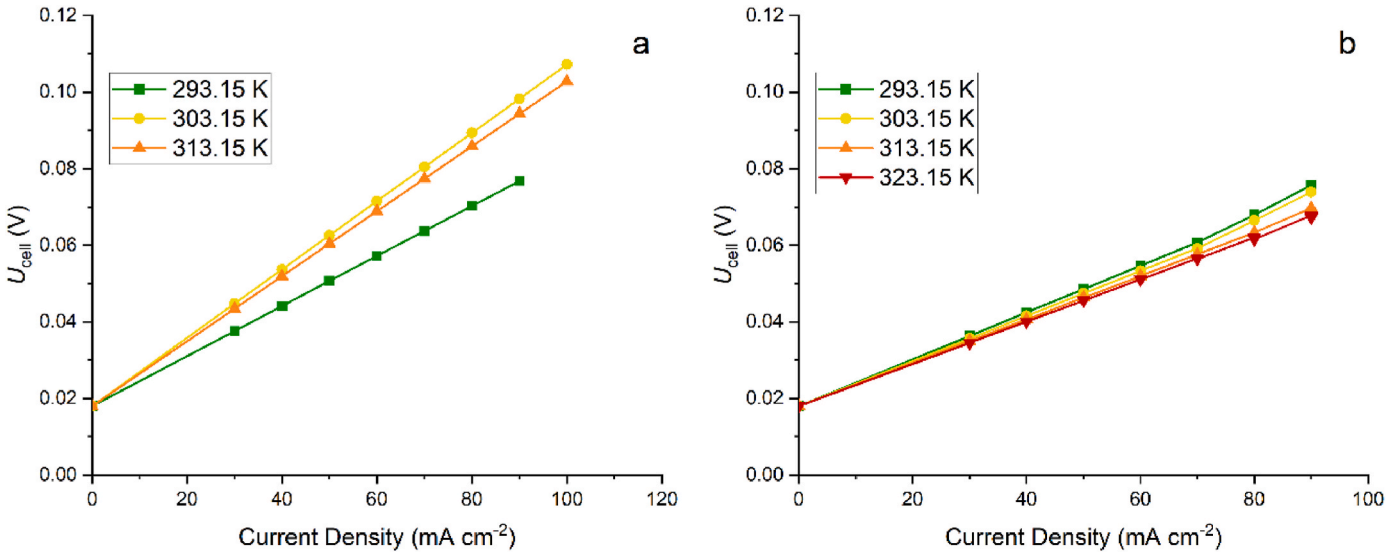

Fig. 5. Polarization curves at different temperature: a) maintaining the same temperature for the cell and the humidifier, b) setting the humidifier 10 K above the cell operating temperature. Process conditions: ambient pressure for cathodic and anodic chambers; hydrogen inner flow 10 NmL·min^{-1}; methane:hydrogen molar ratio 80:20.

Table 4
Resistances obtained from the polarization curves at different temperatures and H_2:CH_4 molar ratio.

H_2:CH_4 molar ratio	Temperature (K)	Resistance (Ω cm)
100:0	293.15	87.6 ± 2.0
	303.15	74.2 ± 1.8
	313.15	71.8 ± 1.4
	323.15	66.8 ± 2.6
30:70	293.15	124.6 ± 1.2
	303.15	105.2 ± 1.6
	313.15	101.4 ± 2.5
	323.15	93.6 ± 2.9
20:80	293.15	130.9 ± 2.3
	303.15	125.9 ± 3.1
	313.15	109.9 ± 0.7
	323.15	90.8 ± 2.2

to the presence of water in the membrane. It is also important to consider that the operating current density is relatively low. Higher current densities would enhance hydrogen flow, the permeation of methane would remain unchanged, as it is not influenced by the current (Equation (11)), increasing the purity.

$$\dot{n}_{i,p} = 3.35{\cdot}10^{-13}{\cdot}k_{Pi}{\cdot}\Delta P_i{\cdot}\frac{A}{L} \quad \text{Eq. 11}$$

where k_{Pi} is the permeability coefficient (barrer), ΔP_i is the partial pressure difference between the two chambers (bar), A is the area of the membrane (cm^2), and L is the thickness of the membrane (cm).

According to this equation using a thicker membrane, like Nafion® 117 can also allow a better separation due to the dependence of methane permeation from the membrane thickness. Another possibility could be working with a membrane that isn't totally wet, indeed the permeation in dry Nafion® is two orders of magnitude lower than that in wet Nafion®. However, both methods would reduce the energy efficiency of the system. An evaluation to quantify how membrane thickness, humidity and current density can reduce methane content to achieve the <100 ppm specification and their impact on energy efficiency was carried out. Among these parameters, membrane humidity appears to have the most significant influence on overall efficiency, as can be seen in Fig. S3 (see Supplementary Material Fig. S3).

3.4. Influence of the temperature

Since it is known that the ionic conductivity of Nafion® increases with temperature, up to a maximum around 333 K [46], the effect of

Table 5
Equations used in the mathematical model.

Parameter	Equation		Ref.
Potential calculation			
Cell potential	$U_{cell} = E + \eta_{ET\ anode} + \eta_{ET\ cathode} + Ri$	Eq. 4	[53]
Nernst potential	$E = E_0 + \frac{R_{gas}T}{nF}\ln\left(\frac{P_{an}{\cdot}x_{H_2,an}}{P_{cat}{\cdot}x_{H_2,cat}}\right)$	Eq. 3	[18]
Butler Volmer[a] Resolution by eqs. 13 and 14	$j = j_0^*{\cdot}C_{H_2}^{\overrightarrow{\alpha}}{\cdot}\left[\exp\left(\frac{\overleftarrow{\alpha}nF\eta_{an}}{R_{gas}T}\right) - \exp\left(-\frac{\overrightarrow{\alpha}nF\eta_{cat}}{R_{gas}T}\right)\right]$	Eq. 12	[18]
Anodic current[a]	$j_{an} = \frac{j + \sqrt{j^2 + 4{\cdot}j_0^{*2}{\cdot}C_{H_2}}}{2}$	Eq. 13	–
Anodic Overpotential[a]	$\eta_{ET\ anode} = \frac{R_{gas}T}{\overleftarrow{\alpha}nF}\ln\left(\frac{j_{an}}{j_0^*\,C_{H_2}^{\overrightarrow{\alpha}}}\right)$	Eq. 14	–
Ohmic resistance	$R = \frac{1}{\sigma}\frac{L}{A}{\cdot}i$	Eq. 8	[21]
Membrane specific conductivity	$\sigma = \sigma_{0(T)}\ max(f_w - 0.06, 0)^{1.5}$	Eq. 15	[54]
Water volume fraction in the membrane	$f_w = \frac{\lambda V_w}{\lambda V_w + V_m}$	Eq. 16	[54]
Membrane equivalent volume	$V_m = \frac{EW}{\rho_{dry}}$	Eq. 17	[55]
Reference membrane conductivity	$\sigma_{0(T)} = \sigma_{0(296\ K)}\exp\left(\frac{1}{296.15} - \frac{1}{T}\right)$	Eq. 18	[21]
Current density	$j = \frac{i}{A}$	Eq. 19	[53]
Material balance			
Surface H_2 molar fraction at the anode	$x_{H_2,an} = x_{H_2,bulk} - i\frac{R_{gas}\,T}{h_m\,P_{an}\,x_{H_2,bulk}\,2\,F}$	Eq. 20	[39]
Hydrogen converted	$\dot{n}_{H_2,i} = \frac{i}{nF}$	Eq. 5	[18]
Gas permeation	$\dot{n}_{i,p} = 3.35{\cdot}10^{-13}{\cdot}k_{Pi}{\cdot}\Delta p_i{\cdot}\frac{A}{L}$	Eq. 11	[18]
Water transport	$\dot{n}_{H_2O} = EOD{\cdot}\frac{i}{F} + D_{H_2O}\frac{\rho_{dry}}{EW{\cdot}L}$	Eq. 21	[55]
Water diffusive coefficient[b]	$D_{H_2O} = \left(5.1\,\lambda - 0.66\lambda^2 + 0.052\lambda^3 - 0.013\lambda^4\right){\cdot}10^{-6}\exp\left[2416\left(\frac{1}{303} - \frac{1}{T}\right)\right]$	Eq. 22	[55]
Membrane water content	$\lambda = \begin{cases} 0.043 + 17.81a_w - 39.85a_w^2 + 36a_w^3 & ;\ 0 \le a_w \le 1 \\ 14 + 1.4(a_w - 1) & ;\ 1 < a_w \le 3 \\ 16.8 & ;\ a_w > 3 \end{cases}$	Eq. 23	[56]
Gas water saturation	$a_w = \frac{p_{H_2O}}{P^0_{H_2O}}$	Eq. 24	[18]
Water vapour pressure	$P^0_{H_2O} = 10^{\left(4.6543 - \frac{1435.264}{T - 64.848}\right)}$	Eq. 25	[57]

[a] Solved independently for each electrode.
[b] As solved by Sdanghi et al. [55] by integrating between the λ calculated at anode and cathode conditions.

temperature on cell performance was also investigated. Three anodic gas mixtures, namely 0:100, 70:30 and 80:20 methane:hydrogen molar ratios, were tested changing the temperature of the cell and the inner gas from 293 to 323 K.

The initial results were unsatisfactory, as no decrease in Ohmic resistance was observed with increasing temperature, contrary to expectations (Fig. 5a). This behaviour could be explained considering that in the membrane-based systems a raise of their temperature can have several negative effects, most notably on the membrane's ability to retain water [27].

To address this issue, the humidifier temperature was set 10 K above the operating temperature of the cell. This modification ensured a higher water content in the gas supplied to the anode chamber, ensuring a constant membrane hydration. Using this configuration, the slope of the polarization curves, and consequently the system's resistance, decreases with an increase in this parameter (Fig. 5b). To better illustrate the temperature effect, the obtained resistances are reported in Table 4.

3.5. Stack configuration of the EHC system

The use of a stack configuration, with more than one cell working, can significantly increase the efficiency and the productivity of the system. The single units are placed electrically in series and in parallel with respect to the gas flow in order to process the required volume flow rate and obtain the desired pressure. So, in a preliminary study presented in this section, a stack of two and three cells was investigated by adding at the electrochemical system bipolar plates and using three MEAs that presents the same characteristics and behaviour of MEA 3.

In this system, where the same current flows through each cell, the total stack resistance is equal to the sum of the single cell resistances, so the stack cell potential, U_{stack}, is the sum of the voltages of the single cells. Indeed, the obtained resistance, equal to 158.2 Ω cm, of the two-cell stack is doubled with respect to the single cell device (87.6 Ω cm), as well as the three-cell stack showed a resistance of 246.5 Ω cm, three times higher than the single cell (see Supplementary Materials Fig. S4). At the same current given to the system, it is possible to purify double or triple quantity of hydrogen, this results in a comparable value of energy consumption per mole of hydrogen. The use of a stack configuration also allows to lower the capital costs and the equipment volume.

4. EHC model

4.1. Model development

A theoretical steady-state model has been developed for the representation of the phenomena involved in the EHC, starting from theoretical and empirical equations that describe the fundamental theory of electrochemical cell processes. It represents an elaboration and application of existing models already present in the literature [39,42–44]. The main goal was to validate the obtained experimental results and to foresee the behaviour of the system described in this work in terms of set up, performance and hydrogen production related to H_2 purity inlet and working conditions. Language C++ was used for the application of the model.

To have a good representation of the internal conditions of the cell, which change significantly in the serpentine of the polar plate, the total area has been divided into portions simulated to calculate the current passing at the potential applied to the cell. Once all the portions are simulated, the total current is obtained as a sum of the single contributions.

Each portion was resolved using an iterative calculation because, even though the potential is the constant parameter throughout the entire cell, it was not possible to calculate the current as a function of it but only the contrary. Starting from a test current, the mass balance between anode and cathode was performed, then the potential was obtained from the anode input and the cathode output conditions. The potential calculated was compared with a target potential: if the calculated one is higher, the current should be lower and vice versa. The calculation is then repeated from the new test current. The illustrative diagram for modelling of electrochemical hydrogen compressor is shown in detail in Fig. S5 (see Supplementary Materials).

Table 6
Parameters of the mathematical model (w.k. = well known value, Exp = specific or obtained during our experiments, Regressed = regressed through our experimental data).

Parameter	Symbol	UOM	Value	Source
Standard potential	E^0	V	0.000	w.k.
Electrons transferred for each H_2	n	–	2	w.k.
Faraday's constant	F	C mol^{-1}	96485	w.k.
Universal gas constant	R_{gas}	J mol^{-1} K^{-1}	8.314	w.k.
Electron transfer symmetry coefficient	$\overleftarrow{\alpha}$, $\overrightarrow{\alpha}$	–	0.5	[56]
Exchange current density at the anode	$j^*_{0,an}$	A cm^{-2}	10	[56]
Exchange current density at the cathode	$j^*_{0,cat}$	A cm^{-2}	11	[56]
Nafion conductivity at 296.15 K	$\sigma_{0(296\ K)}$	S cm^{-1}	0.072	Regressed
Water molar volume	V_w	m^3 mol^{-1}	$1.8{\cdot}10^{-5}$	w.k.
Mass transfer coefficient for the GDL	h_m	L s^{-1} cm^{-2}	0.1	Regressed
Electro-osmotic drag coefficient	EOD	–	0.9	[56]
Permeability coefficient	k_p	Barrer	Different value	Exp (see Section 3.3)
Thickness of the membrane	L	cm	Different value	Table 2
Area of the membrane	A	cm^2	10	Exp
Equivalent weight of the membrane	EW	kg mol^{-1}	Different value	Table 2
Dry membrane density	ρ_{dry}	kg m^{-3}	Different value	Table 2

The model for a single area portion has been developed from the equations listed in Table 5 and the parameters in Table 6.

The simulated results of this work were obtained considering the cell divided in 1000 equal portions. This resolution was chosen since, at this level of discretization, the results could be considered independent of the number of sections used.

4.2. Results and discussion

Thanks to the portioning of the area, it was possible also to evaluate the flux limited current, as well as the corresponding overpotentials, without inserting an equation to describe them.

The electrochemical behaviour of investigated MEA 1, 2 and 3 was well fitted by the model (Fig. 6a), and the model was also able to well represent the polarization curves of the cell used with different composition of anodic gas mixtures (Fig. 6b), starting from the equilibrium potential in agreement with the experimentally measured at OCP, to the change in slope due to flux limitations in the region near the flux limited current, already discussed in Section 3.1.

The rise in U_{cell} resulting from hydrogen depletion along the serpentine flow field, previously presented in Section 3.3, was examined in greater detail. This investigation focused on the interplay between reactant distribution and electrochemical performance, highlighting how the progressive consumption of hydrogen along the flow path leads to localized increases in overpotential. The variation in current density across 1000 simulated active areas revealed a clear correlation with the reduction in hydrogen flow caused by its gradual transport to the cathode chamber (see Supplementary Materials Fig. S6). This effect is more pronounced at higher current densities (see Supplementary Materials Figs. S7–S9), where the hydrogen depletion is greater, leading to

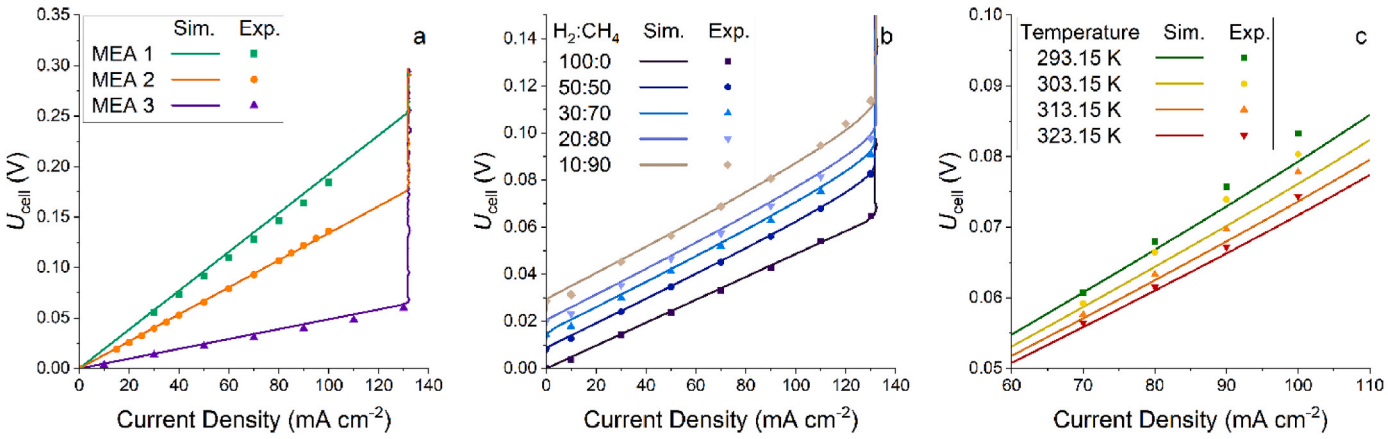

Fig. 6. Comparison between simulated and experimental results for a) different membranes, b) different hydrogen-methane concentrations and c) different temperatures.

a more significant increase in U_{cell} in these regions. The localized variation of current density at lower hydrogen concentrations is caused by the balance between the increase of the equilibrium potential (E) and the decrease of the Ohmic overpotential (iR).

Finally, the U_{cell} temperature dependence was simulated reproducing some polarization curves at different temperature. Also in this case a good correlation was obtained as can be seen in Fig. 6c. The experimental variation is greater than the simulated one, but this result could be explained by the fact that the membrane humidification control is difficult at high temperatures, and this could lead to higher Ohmic overpotentials [27].

In conclusion, the model was able to fit the experimental data and could be used to make reliable previsions on the electrochemical performances of the EHC with an average deviation from all the experimental data of 2.51 %, calculated using Equation (26). In Table S1 (see Supplementary Materials) are reported all the average deviations between experimental and simulated data for every simulation set.

$$\delta = \left|U_{cell,\ exp} - U_{cell,\ sim}\right| / U_{cell,\ exp} \qquad \text{Eq. 26}$$

where $U_{cell\ exp}$ is the experimental value of cell potential and $U_{cell\ sim}$ is the simulated one at the same conditions. In addition thanks to the collected data regarding the membrane permeation of methane and hydrogen, it was possible to add to the model the calculation of the hydrogen purity and system efficiency, which were in accordance to the values experimentally obtained.

5. Conclusion

The purification of hydrogen from a methane-hydrogen mixture was studied to evaluate a possible procedure to separate this energy carrier from the natural gas pipelines. Electrochemical Hydrogen Compressor (EHC) can be considered a suitable system for hydrogen separation from methane, especially in the case of small units of separation. Since what affects the efficiency of this device is the Ohmic resistance of the system, which can be mainly attributed to the cationic membrane, three different Nafion® membranes were studied. From the energy efficiency point of view the best membrane is Nafion® 212 which presents the lowest thickness and the higher ion-exchange capacity. On this membrane, the influence on the cell performance of different concentration of methane, fed to the anodic chamber and temperature were evaluated. Results highlight that, when hydrogen is purified from a stream with a 90:10 methane:hydrogen molar ratio, the energy consumption only slightly increases from 1.20 kWh·kgH_2^{-1}, when there is only hydrogen in the stream, to 2.30 kWh· kgH_2^{-1}. In addition, only a weak increase of Ohmic resistance of the system was revealed, due to diffusional limitation. The purity of the hydrogen obtained from a 90:10 methane: hydrogen mixture can reach very high values, up to 99.45 %, but not enough to meet the regulatory values for fuel cells, which ask for a CH_4 content of less than 100 ppm. Using higher current density, a thicker membrane, like Nafion® 117, or working with a membrane that isn't totally wet are three ways to get around this issue, although the last two methods will reduce energy efficiency. It has also been shown how the increase of the temperature allows a slight lowering of the resistance thanks to the increase of conductivity of the membrane. However, it should be mentioned that raising the system's temperature can have negative effects, most notably on the water management of the membrane and an increase in the total energy consumption of the system due to the heating system. The results also demonstrated the feasibility of reducing the amount of the precious Pt in the anode without compromising cell performance in terms of both potential and separation efficiency. All the experimental results were validated with a mathematical, achieving an average deviation of 2.5 % between the model and experimental data.

CRediT authorship contribution statement

Elisa Zanella: Writing – review & editing, Writing – original draft, Visualization, Validation, Supervision, Software, Methodology, Investigation, Formal analysis, Data curation, Conceptualization. **Mariangela Longhi:** Writing – review & editing, Validation, Supervision, Project administration, Data curation, Conceptualization. **Giacomo Tondelli:** Writing – review & editing, Writing – original draft, Visualization, Validation, Software, Methodology, Investigation, Formal analysis, Data curation, Conceptualization. **Alessandro Minguzzi:** Writing – review & editing. **Antonio Comite:** Writing – review & editing, Validation, Supervision, Resources, Methodology, Conceptualization. **Alberto Vertova:** Writing – review & editing, Validation, Supervision, Methodology, Conceptualization. **Carlo Pirola:** Writing – review & editing, Supervision, Resources, Project administration, Methodology, Funding acquisition, Conceptualization.

Declaration of competing interest

The authors declare that they have no known competing financial interests or personal relationships that could have appeared to influence the work reported in this paper.

Acknowledgements

This project was co-funded with resources in the frame of the PON REACT-EU financing Program Action IV.5 – Doctorates on green topics.

A.M. is grateful to a project funded under the National Recovery and

Resilience Plan (NRRP), Mission 4 Component 2 Investment 1.3 - Call for tender No. 1561 of 11.10.2022 of Ministero dell'Università e della Ricerca (MUR); funded by the European Union – NextGenerationEU Project code PE0000021, Concession Decree No. 1561 of 11.10.2022 adopted by Ministero dell'Università e della Ricerca (MUR), CUP D43C22003090001, Project title "Network 4 Energy Sustainable Transition – NEST".

Appendix A. Supplementary data

Supplementary data to this article can be found online at https://doi.org/10.1016/j.ijhydene.2025.04.014.

References

[1] International Energy Agency (IEA). World energy outlook 2024. 2024.
[2] Hydrogen. In: Energy for a sustainable world; 2010. p. 279–99. https://doi.org/10.1002/9783527633593.ch14.
[3] Pareek A, Dom R, Gupta J, Chandran J, Adepu V, Borse PH. Insights into renewable hydrogen energy: recent advances and prospects. Mater Sci Energy Technol 2020;3:319–27. https://doi.org/10.1016/j.mset.2019.12.002.
[4] Ahluwalia RK, Peng JK. Automotive hydrogen storage system using cryo-adsorption on activated carbon. Int J Hydrogen Energy 2009;34:5476–87. https://doi.org/10.1016/j.ijhydene.2009.05.023.
[5] EU Monitor. Communication COM/2020/301: a hydrogen strategy for a climate-neutral Europe, ommunication from the commission to the European parliament, the council, the European economic and social committee and the committee of the regions 53. 2020.
[6] European hydrogen Backbone. https://ehb.eu/page/european-hydrogen-backbone-maps. [Accessed 14 October 2024].
[7] Makaryan IA, V Sedov I, Salgansky EA, V Arutyunov A, Arutyunov VS. A comprehensive review on the prospects of using hydrogen–methane blends: challenges and opportunities. Energies 2022;15:2265.
[8] Abbas HF, Wan Daud WMA. Hydrogen production by methane decomposition: a review. Int J Hydrogen Energy 2010;35:1160–90. https://doi.org/10.1016/j.ijhydene.2009.11.036.
[9] Król A, Gajec M, Holewa-Rataj J, Kukulska-Zając E, Rataj M. Hydrogen purification technologies in the context of its utilization. Energies 2024;17:3794.
[10] Sircar S, Golden TC. Pressure swing adsorption technology for hydrogen production, Hydrogen and Syngas Production and Purification. Technologies 2009;10:414–50.
[11] Dehdari L, Burgers I, Xiao P, Li KG, Singh R, Webley PA. Purification of hydrogen from natural gas/hydrogen pipeline mixtures. Sep Purif Technol 2022;282:120094. https://doi.org/10.1016/j.seppur.2021.120094.
[12] Jackson C, Smith G, Kucernak AR. Deblending and purification of hydrogen from natural gas mixtures using the electrochemical hydrogen pump. Int J Hydrogen Energy 2024;52:816–26. https://doi.org/10.1016/j.ijhydene.2023.05.065.
[13] Al-Mufachi NA, V Rees N, Steinberger-Wilkens R. Hydrogen selective membranes: a review of palladium-based dense metal membranes. Renew Sustain Energy Rev 2015;47:540–51. https://doi.org/10.1016/j.rser.2015.03.026.
[14] Bernardo G, Araújo T, da Silva Lopes T, Sousa J, Mendes A. Recent advances in membrane technologies for hydrogen purification. Int J Hydrogen Energy 2020;45:7313–38. https://doi.org/10.1016/j.ijhydene.2019.06.162.
[15] Bastani D, Esmaeili N, Asadollahi M. Polymeric mixed matrix membranes containing zeolites as a filler for gas separation applications: a review. J Ind Eng Chem 2013;19:375–93. https://doi.org/10.1016/j.jiec.2012.09.019.
[16] Rohland B, Eberle K, Ströbel R, Scholta J, Garche J. Electrochemical hydrogen compressor. Electrochim Acta 1998;43:3841–6. https://doi.org/10.1016/S0013-4686(98)00144-3.
[17] Sdanghi G, Maranzana G, Celzard A, Fierro V. Review of the current technologies and performances of hydrogen compression for stationary and automotive applications. Renew Sustain Energy Rev 2019;102:150–70. https://doi.org/10.1016/j.rser.2018.11.028.
[18] Chouhan A, Bahar B, Prasad AK. Effect of back-diffusion on the performance of an electrochemical hydrogen compressor. Int J Hydrogen Energy 2020;45:10991–9. https://doi.org/10.1016/j.ijhydene.2020.02.048.
[19] Rhandi M, Trégaro M, Druart F, Deseure J, Chatenet M. Electrochemical hydrogen compression and purification versus competing technologies: Part I. Pros and cons. Chin J Catal 2020;41:756–69. https://doi.org/10.1016/S1872-2067(19)63404-2.
[20] Ströbel R, Oszcipok M, Fasil M, Rohland B, Jörissen L, Garche J. The compression of hydrogen in an electrochemical cell based on a PE fuel cell design. J Power Sources 2002;105:208–15. https://doi.org/10.1016/S0378-7753(01)00941-7.
[21] Marciuš D, Kovač A, Firak M. Electrochemical hydrogen compressor: recent progress and challenges. Int J Hydrogen Energy 2022;47:24179–93. https://doi.org/10.1016/j.ijhydene.2022.04.134.
[22] Durmus GNB, Colpan CO, Devrim Y. A review on the development of the electrochemical hydrogen compressors. J Power Sources 2021;494:229743. https://doi.org/10.1016/j.jpowsour.2021.229743.
[23] Fracchia M, Ghigna P, Marelli M, Scavini M, Vertova A, Rondinini S, Della Pergola R, Minguzzi A. Molecular cluster route for the facile synthesis of a stable and active Pt nanoparticle catalyst. New J Chem 2021;45:11292–303. https://doi.org/10.1039/D1NJ00937K.
[24] Minelli S, Civelli M, Rondinini S, Minguzzi A, Vertova A. AEMFC exploiting a Pd/CeO2-based anode compared to classic PEMFC via LCA analysis. Hydro 2021;2:246–61. https://doi.org/10.3390/hydrogen2030013.
[25] Zou J, Han N, Yan J, Feng Q, Wang Y, Zhao Z, Fan J, Zeng L, Li H, Wang H. Electrochemical compression technologies for high-pressure hydrogen: current status, challenges and perspective. Electrochem Energy Rev 2020;3:690–729.
[26] Chiou JS, Paul DR. Gas permeation in a dry Nafion membrane. Ind Eng Chem Res 1988;27:2161–4. https://doi.org/10.1021/ie00083a034.
[27] Pineda-Delgado JL, Chávez-Ramirez AU, Gutierrez B CK, Rivas S, Marisela C-R, de Jesús Hernández-Cortes R, Menchaca-Rivera JA, Pérez-Robles JF. Effect of relative humidity and temperature on the performance of an electrochemical hydrogen compressor. Appl Energy 2022;311:118617. https://doi.org/10.1016/j.apenergy.2022.118617.
[28] Perry KA, Eisman GA, Benicewicz BC. Electrochemical hydrogen pumping using a high-temperature polybenzimidazole (PBI) membrane. J Power Sources 2008;177:478–84. https://doi.org/10.1016/j.jpowsour.2007.11.059.
[29] Durmuş GNB, Colpan CO, Devrim Y. Investigation of the performance of high-temperature electrochemical hydrogen purification from reformate gases. Int J Energy Res 2022;46:11443–55.
[30] Jackson C, Raymakers LFJM, Mulder MJJ, Kucernak ARJ. Assessing electrocatalyst hydrogen activity and CO tolerance: comparison of performance obtained using the high mass transport 'floating electrode' technique and in electrochemical hydrogen pumps. Appl Catal, B 2020;268:118734. https://doi.org/10.1016/j.apcatb.2020.118734.
[31] Grigoriev SA, Shtatniy IG, Millet P, Porembsky VI, Fateev VN. Description and characterization of an electrochemical hydrogen compressor/concentrator based on solid polymer electrolyte technology. Int J Hydrogen Energy 2011;36:4148–55. https://doi.org/10.1016/j.ijhydene.2010.07.012.
[32] Nguyen M-T, Grigoriev SA, Kalinnikov AA, Filippov AA, Millet P, Fateev VN. Characterisation of a electrochemical hydrogen pump using electrochemical impedance spectroscopy. J Appl Electrochem 2011;41:1033–42. https://doi.org/10.1007/s10800-011-0341-9.
[33] Chouhan A, Aryal UR, Sivakumar PO, Bahar B, Prasad AK. Challenges in the electrochemical compression of an ammonia-hydrogen blend. Int J Hydrogen Energy 2021;46:37965–76. https://doi.org/10.1016/j.ijhydene.2021.09.076.
[34] Jackson C, Raymakers LFJM, Mulder MJJ, Kucernak ARJ. Poison mitigation strategies for the use of impure hydrogen in electrochemical hydrogen pumps and fuel cells. J Power Sources 2020;472:228476. https://doi.org/10.1016/j.jpowsour.2020.228476.
[35] Ibeh B, Gardner C, Ternan M. Separation of hydrogen from a hydrogen/methane mixture using a PEM fuel cell. Int J Hydrogen Energy 2007;32:908–14. https://doi.org/10.1016/j.ijhydene.2006.11.017.
[36] Onda K, Ichihara K, Nagahama M, Minamoto Y, Araki T. Separation and compression characteristics of hydrogen by use of proton exchange membrane. J Power Sources 2007;164:1–8. https://doi.org/10.1016/j.jpowsour.2006.10.018.
[37] Doucet R, Gardner CL, Ternan M. Separation of hydrogen from hydrogen/ethylene mixtures using PEM fuel cell technology. Int J Hydrogen Energy 2009;34:998–1007. https://doi.org/10.1016/j.ijhydene.2008.10.069.
[38] Thomassen M, Sheridan E, Kvello J. Electrochemical hydrogen separation and compression using polybenzimidazole (PBI) fuel cell technology. J Nat Gas Sci Eng 2010;2:229–34. https://doi.org/10.1016/j.jngse.2010.10.002.
[39] Nordio M, Rizzi F, Manzolini G, Mulder M, Raymakers L, Van Sint Annaland M, Gallucci F. Experimental and modelling study of an electrochemical hydrogen compressor. Chem Eng J 2019;369:432–42. https://doi.org/10.1016/j.cej.2019.03.106.
[40] Vermaak L, Neomagus HWJP, Bessarabov DG. Hydrogen separation and purification from various gas mixtures by means of electrochemical membrane technology in the temperature range 100–160 °C. Membranes 2021;11. https://doi.org/10.3390/membranes11040282.
[41] Karimi MB, Mohammadi F, Hooshyari K. Recent approaches to improve Nafion performance for fuel cell applications: a review. Int J Hydrogen Energy 2019;44:28919–38. https://doi.org/10.1016/j.ijhydene.2019.09.096.
[42] Prokopou GI, Mödden ML, Mitsos A, Bongartz D. Optimal sizing and operation of electrochemical hydrogen compression. Chem Eng Sci 2024;293:120031. https://doi.org/10.1016/j.ces.2024.120031.
[43] Aziz M, Aryal UR, Prasad AK. Optimization of electrochemical hydrogen compression through computational modeling. Int J Hydrogen Energy 2022;47:33195–208. https://doi.org/10.1016/j.ijhydene.2022.07.256.
[44] Marciuš D, Kovač A, Firak M. Fundamental mathematical model of electrochemical hydrogen compressor. Energy Convers Manag 2024;309:118423. https://doi.org/10.1016/j.enconman.2024.118423.
[45] Zanella E, Tonsi G, Grainca A, Jamoletti F, Longhi M, Pirola C. Hydrogen purification and odorization to evaluate the distribution of this energy carrier through the gas pipelines. Chem Eng Trans 2023;105:61–6. https://doi.org/10.3303/CET23105011.
[46] Yadav R, Fedkiw PS. Analysis of EIS technique and Nafion 117 conductivity as a function of temperature and relative humidity. J Electrochem Soc 2012;159:B340.
[47] Nafion™ membranes. https://www.nafion.com/en; 2024.
[48] Xu T. Ion exchange membranes: state of their development and perspective. J Membr Sci 2005;263:1–29. https://doi.org/10.1016/j.memsci.2005.05.002.
[49] International organization for standardization. ISO 14687:2019 Hydrogen fuel quality - product specification. 2019.
[50] Schalenbach M, Hoefner T, Paciok P, Carmo M, Lueke W, Stolten D. Gas permeation through nafion. Part 1: measurements. J Phys Chem C 2015;119:25145–55. https://doi.org/10.1021/acs.jpcc.5b04155.

[51] Mukaddam M, Litwiller E, Pinnau I. Gas sorption, diffusion, and permeation in nafion. Macromolecules 2016;49:280–6. https://doi.org/10.1021/acs.macromol.5b02578.
[52] Fan Y, Tongren D, Cornelius CJ. The role of a metal ion within Nafion upon its physical and gas transport properties. Eur Polym J 2014;50:271–8. https://doi.org/10.1016/j.eurpolymj.2013.11.011.
[53] Schmickler W, Santos E. Phenomenological treatment of electron-transfer reactions. In: Schmickler W, Santos E, editors. Interfacial electrochemistry. Berlin, Heidelberg: Springer Berlin Heidelberg; 2010. p. 91–8. https://doi.org/10.1007/978-3-642-04937-8_9.
[54] Weber AZ, Newman J. Transport in polymer-electrolyte membranes : II. Mathematical model. J Electrochem Soc 2004;151:A311. https://doi.org/10.1149/1.1639157.
[55] Sdanghi G, Dillet J, Didierjean S, Fierro V, Maranzana G. Feasibility of hydrogen compression in an electrochemical system: focus on water transport mechanisms. Fuel Cells 2020;20:370–80. https://doi.org/10.1002/fuce.201900068.
[56] Toghyani S, Baniasadi E, Afshari E, Javani N. Performance analysis and exergoeconomic assessment of a proton exchange membrane compressor for electrochemical hydrogen storage. Int J Hydrogen Energy 2020;45:34993–5005. https://doi.org/10.1016/j.ijhydene.2020.01.232.
[57] Stull DR. Vapor pressure of pure substances. Organic and inorganic compounds. Ind Eng Chem 1947;39:517–50. https://doi.org/10.1021/ie50448a022.